

See discussions, stats, and author profiles for this publication at: <https://www.researchgate.net/publication/225188278>

# Miscibility, Crystallinity, and Phase Development in P3HT/PCBM Solar Cells: Toward an Enlightened Understanding of Device Morphology and Stability

ARTICLE in JOURNAL OF PHYSICAL CHEMISTRY LETTERS · DECEMBER 2011

Impact Factor: 7.46 · DOI: 10.1021/jz2014902

---

CITATIONS

139

READS

328

## 3 AUTHORS, INCLUDING:



[Brian Akira Collins](#)

National Institute of Standards and Technology

48 PUBLICATIONS 1,044 CITATIONS

[SEE PROFILE](#)



[Harald Werner Ade](#)

North Carolina State University

356 PUBLICATIONS 8,667 CITATIONS

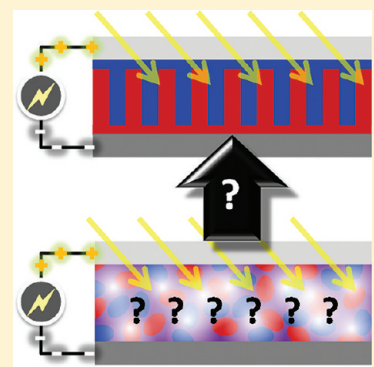
[SEE PROFILE](#)

# Miscibility, Crystallinity, and Phase Development in P3HT/PCBM Solar Cells: Toward an Enlightened Understanding of Device Morphology and Stability

Brian A. Collins, John R. Tumbleston, and Harald Ade\*

Department of Physics, North Carolina State University, North Carolina

**ABSTRACT:** Rapid improvements in organic solar cell efficiency have brought these devices into the spotlight as a potential source of abundant electricity. Despite much empirical progress, fundamental understanding is still lacking. Due to the required three-dimensional nanoscale morphology, determining structure–performance relationships has been a major challenge, and a convergent understanding has yet to emerge. We discuss recent major advances in delineating the characteristics of the most common organic solar cells. The large variations in device performance reported, the contradictory morphologies observed, and the determination of the underlying driving forces need to be resolved. Deeper understanding that can provide a roadmap to improved devices will only occur through refined consideration of material characteristics and fabrication procedures in conjunction with increased use of advanced characterization. We additionally highlight the recently discovered partial miscibility of the component materials, its influence on device processing and lifetime, and its emergence as an important indicator of stability.



The encouragingly rapid improvement of organic photovoltaic (OPV) devices in recent years has brought significant attention to their potential to become an economically viable source of cheap, renewable electrical energy. The simple solution processing methods and relatively inexpensive materials used in these devices allow for swift roll-to-roll large-scale production, affording OPVs the potential of being more cost-effective and flexible in application than their more established inorganic counterparts. Determined early research on the mechanism of photoconversion in OPVs seeded a revolution in research and development, resulting in power conversion efficiencies (PCEs) exceeding 8%.<sup>1</sup> The basic photoconversion model established that photon absorption generates a short-lived bound exciton (electron/hole pair), which must be separated at a donor–acceptor material interface within ~10 nm to avoid energy loss through recombination. However, the absorbing layer must be on the order of hundreds of nanometers thick for efficient absorption. These competing length scales led to the development of the bulk heterojunction (BHJ) concept of two interpenetrating nanoscale phases, where exciton separation occurred throughout the bulk of the active layer instead of at a single interface in the case of more primitive bilayer devices.<sup>2,3</sup> This BHJ paradigm conceptualized discrete donor–acceptor interfaces for efficient exciton dissociation along with pure, interdigitated, nanoscale phases for efficient charge-transport pathways to the electrodes. This architecture was partially realized by casting the donor and acceptor materials from a common solution where phase separation was induced by various means, resulting in the morphological description exemplified in Figure 1a. On the basis of this model, a comb-like structure with phases ordered perpendicular to the substrate and appropriate interface wetting

layers was envisioned as the ideal morphology in these devices.<sup>4,5</sup>

Although discrete interfaces between ~10 nm pure domains randomly organized in the BHJ have been canonical assumptions of actual device morphology for some time, even this description has recently been proven far too simple to describe real devices. Despite years of research and over 1000 publications, a consensus view has not yet emerged for even the most studied material system, poly(3-hexylthiophene) (P3HT) and phenyl-C61-butyric acid methyl ester (PCBM) (chemical structures in Figure 1). Discordant views exist of the precise morphology, the equilibrium phase diagram, vertical segregation, and the mechanism by which phase separation occurs. Contradicting claims and explanations abound in the literature. For example, arguments in favor of crystallization,<sup>6,7</sup> spinodal decomposition,<sup>8</sup> or PCBM agglomeration<sup>9</sup> as the driver of phase separation have been proposed. Similarly, following the initial indication of partial miscibility of PCBM in P3HT by Watts et al.,<sup>10</sup> and the subsequent confirmation by a number of studies,<sup>6,11–14</sup> discussions have emerged on how many phases exist in actual P3HT/PCBM devices and what functional role these phases play. Recent work on other systems even suggests that domains need not be uniformly ~10 nm in size but that morphologies with a hierarchy of length scales can produce efficient devices.<sup>15</sup>

In this Perspective, we will illustrate the evolution of BHJ morphological properties and the ensuing agreements and disagreements by discussing representative examples from the literature. We frequently find that an important aspect to

Received: November 10, 2011

Accepted: November 23, 2011

Published: November 23, 2011

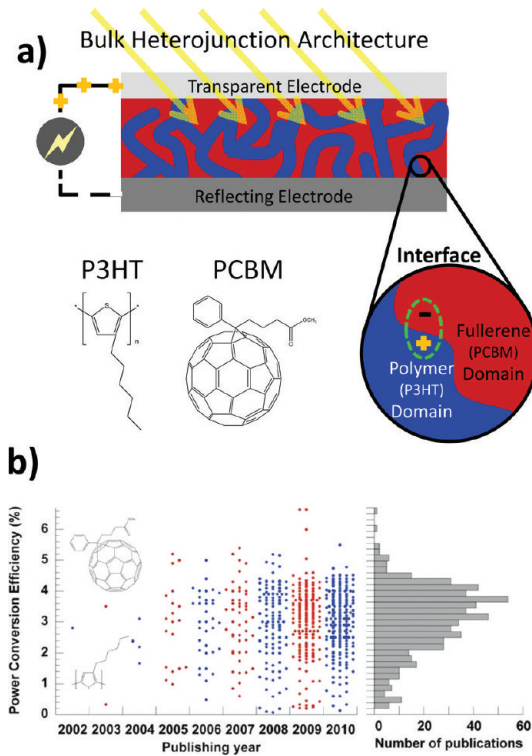


**Figure 1.** State and evolution of the field. (a) Common schematic of the original bulk heterojunction solar cell paradigm, which consisted of two pure, randomly organized and interpenetrating domains. P3HT and PCBM chemical structures are inset along with a zoom of a charge-transfer state at a material interface. (b) Scatter plot of literature reported power conversion efficiency for P3HT/PCBM devices with time. Image (b) is taken from ref 17, adapted with permission from Wiley, copyright 2011.

understanding discrepancies is the careful consideration of the sample preparation methods and materials used. Exacting details about the materials and processing methods is even more relevant when considering systems other than P3HT/PCBM, for which morphologies are significantly altered under the influence of percent levels of solvent additives. Although none of these material systems have morphologies fitting the original BHJ paradigm or are fabricated with the idealized interdigitated comb-like architecture, many exhibit high quantum efficiencies and fill factors with minimal photocurrent losses. This challenges whether the originally envisioned BHJ morphology is actually required to yield high performance. More fundamentally, the final device morphology and long-term stability of the cells are highly influenced by the underlying physical chemistry principles of miscibility of the active components in a given solvent, their miscibility with each other, the ability and propensity of the active components to crystallize, and the interfacial energies with the electrode interfaces.

Not surprisingly and completely analogous with the discordant views on the structures and mechanisms driving their evolution, the reported efficiencies for P3HT/PCBM devices continue to exhibit a large spread that is not converging (see Figure 1b); although, an upper bound of ~4.5% has emerged with very few outliers. Results can depend on rather subtle variables rarely reported in the literature, such as the age of the solution mixture causing the formation of material aggregates and/or solvent levels in the deposition environment.<sup>16</sup> Often, good device performance cannot be repeated easily even in the same lab when a new batch of materials is

sourced. Additionally, studies that use advanced characterization techniques and report new morphological insights rarely correlate them directly with device characteristics, and if they do, they often report PCEs < 2–3%, calling into question the applicability of the results in relation to optimized devices. To answer important morphological questions and definitively connect morphology to device performance, just as much attention should be given to preparation of device-relevant samples as to the advanced characterization techniques applied to them. This will likely require increased collaboration between research groups specializing in material synthesis, device measurement, and structural characterization in efforts to share samples and expertise in a “round-robin” approach. Only through careful, simultaneous attention to materials synthesis, sample processing, and advanced characterization techniques can the field continue to eliminate contradictory results and resolve structure–performance relationships.

Unfortunately, many of the initially utilized characterization tools to investigate morphology have known limitations. For example, scanning probe microscopy only exhibits surface sensitivity, while interpretations of defocused TEM data have been cited as controversial.<sup>18</sup> Obtaining answers to the fundamental morphological questions mentioned above has only recently been made possible with the development of more sophisticated characterization techniques. Among these are advanced scattering methods that require large-scale facilities such as neutron or synchrotron radiation sources as well as advanced electron microscopy methods using energy filtering. While scattering provides statistical information on general structural ordering and crystallinity, microscopy delivers local information such as specific phase identification, which makes these methods ideal compliments to one another. For P3HT/PCBM devices, significant advancements in characterizing the morphology have been made using both classes of techniques.

**Time-Resolved Evolution of Morphology through Scattering.** In general, scattering has determined several important morphological attributes of P3HT/PCBM, including phase separation and crystal population, size, and orientation. P3HT crystallinity in P3HT/PCBM blends has been shown by grazing incidence wide-angle X-ray scattering (GIWAXS) to depend on various parameters including molecular weight, regioregularity,<sup>19</sup> casting solvent,<sup>20</sup> and thermal annealing. Given the dramatic increase in device performance upon thermal treatment that is coincident with enhanced hole mobility<sup>21</sup> and reduced bimolecular recombination,<sup>22</sup> the extent of crystallization of both components during BHJ annealing has been a primary topic of numerous studies. Furthermore, the development of intense synchrotron radiation sources and rapid data acquisition has recently allowed for studies of crystallization and phase separation dynamics on the time scale of seconds. Starting with spun-cast films with relatively low crystallinity, enhancements in the crystal population and size of P3HT is observed, as shown in Figure 2a,b. Multiple studies agree that this crystallization occurs rapidly (<5 min.)<sup>7,9,23</sup> and results in a predominately edge-on configuration, as diagramed in Figure 2d, for which the alkyl side chains are mostly perpendicular to the substrate. Even though *in situ* device performance measurements during annealing and solvent drying show improved performance over time,<sup>7,24</sup> the morphology may not be optimized, as evidenced by PCEs < 2.0%.<sup>7,25</sup>

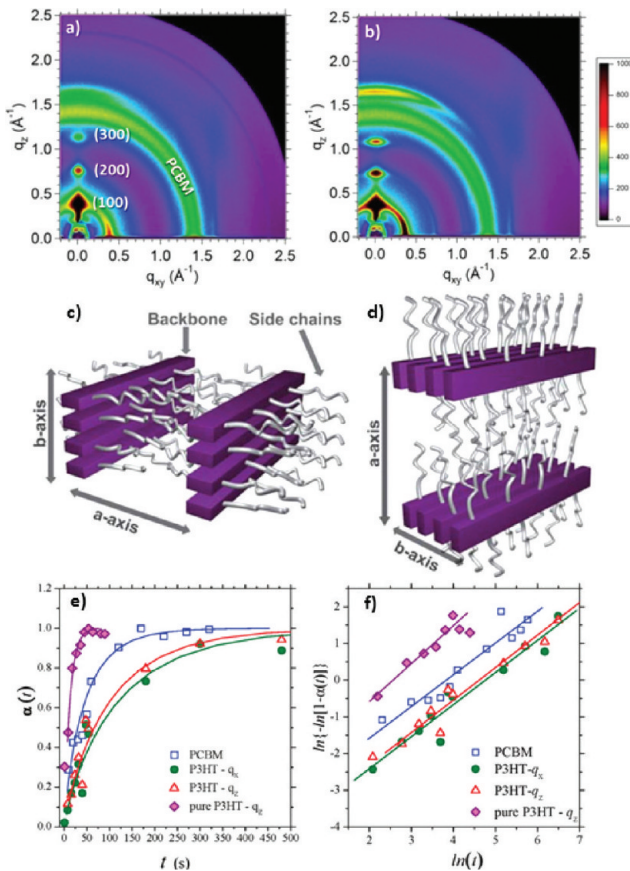


**Figure 2.** In situ X-ray scattering. GIWAXS scattering patterns measuring in situ crystallization for P3HT/PCBM (a) as cast and (b) after 5 min of annealing at 90 °C. The configuration of P3HT chains is predominately (d) edge-on compared to (c) face-on after annealing. (e,f) In the BHJ, P3HT is shown to crystallize on a slower time scale compared to the evolution of phase separation (labeled as “PCBM”), as evidenced by simultaneous GISAXS. Images (a–d) are taken from ref 24, adapted with permission from RSC, copyright 2011. Images (e) and (f) are taken from ref 9.

Unlike the crystal population and size, the *d*-spacing of P3HT crystal planes in pure P3HT and blended films remains constant under annealing. This indicates that pure P3HT crystals tens of nm in size and with minimal PCBM intercalation comprise one phase of the P3HT/PCBM morphology.<sup>11</sup> Given the existence of pure P3HT crystals, it would not be surprising if pure PCBM crystals of similar size also existed, which would correspond to or at least corroborate the pure-phase BHJ morphological model. PCBM crystals were in fact observed for ultrathin<sup>26</sup> and ultrathick blend films in scattering measurements.<sup>27</sup> However, other GIWAXS studies<sup>7,24,28,29</sup> have not observed PCBM crystals, supposedly due to the use of ~100 nm thick films more comparable to those used in devices. Instead of PCBM crystals, amorphous PCBM is observed, as indicated by the broad halo in Figure 2a,b at  $q = 1.4 \text{ \AA}^{-1}$ . Fundamentally, it is unclear how PCBM crystallization would be suppressed for ~100 nm thick films and not for both thinner and thicker active layers.

In order to probe the larger-scale phase separation of P3HT and PCBM, grazing incidence small-angle X-ray scattering (GISAXS) has been employed. Recently, simultaneous and time-resolved GIWAXS/GISAXS measurements have been conducted during in situ annealing to probe both the crystallization and phase separation of P3HT and PCBM.<sup>9</sup>

It was found by comparing pure and blend films that P3HT crystallization was hampered in the presence of PCBM, a result confirmed by other X-ray studies.<sup>7,28</sup> This work also indicates that phase separation occurs on a faster time scale than P3HT crystallization, as shown in Figure 2e,f (phase separation denoted as “PCBM”). The authors argue that phase separation competes favorably with P3HT crystallization under thermal annealing. However, this is not the conclusion reached from other in situ annealing GIWAXS experiments, where it is argued that P3HT crystallization is the driving force of phase separation.<sup>7,28</sup> Further studies will likely be necessary, but as discussed below, fundamental measurements of miscibility and equilibrium may help resolve this open question.

Along with X-ray scattering, small-angle neutron scattering (SANS) has been increasingly used to probe the phase separation in P3HT/PCBM blends. However, major discrepancies have arisen in the data and interpretation for both SANS and GISAXS. Figure 3 shows the variability in scattering profiles obtained for as-cast and annealed P3HT/PCBM BHJs and interdiffused bilayers (Figure 3g). Even though the scattering intensity universally increases under annealing for both X-ray<sup>9,30–32</sup> (Figure 3a–d) and neutron<sup>6,14,23,33</sup> (Figure 3e–h) measurements, scattering peaks are sometimes noted at roughly 0.02  $\text{\AA}^{-1}$  (Figure 3b–g) and sometimes not (Figure 3a,h). As with GIWAXS, differences may occur due to variations in sample preparation as neutron scattering requires either drop-cast films<sup>33</sup> or stacks of multiple samples in the form of either laminated bilayers<sup>23</sup> or blend films<sup>6,14</sup> to achieve meaningful signal. This can limit the applicability to actual devices, especially in the case of drop-cast films, which dry more slowly than spin-cast films. Likewise, films studied are not always cast from solvents used in devices. Yin and Dadmum, for example, use dichloromethane,<sup>33</sup> which has been shown to be a preferential PCBM solvent.<sup>34</sup> The choice of substrate has also not been consistent with devices<sup>9,30,33</sup> even though substrate polarity can significantly affect the morphology and the propensity for PCBM to crystallize.<sup>35</sup> These discrepancies highlight important aspects of sample preparation that are likely a major source of variation in the data and a contributing cause for possible confusion in the field.

Aside from variations in the data, interpretations of the origins of scattering intensities differ; it has been argued that either PCBM agglomeration<sup>9,14,30,31</sup> or P3HT crystals<sup>33</sup> in a uniform mixed matrix are the source of the observed scattering features. Assignment of the source of a particular scattering feature to a specific material and morphology is difficult, since pure P3HT crystals embedded in a mixed phase would have similar scattering contrast and cause similar scattering patterns as PCBM agglomerates in a mixed phase. This can be understood considering a generalized Babinet’s principle since only amplitudes are preserved in scattering. Furthermore, detailed interpretation of scattering data requires the use of a model, the choice of which depends on the assumptions made about the underlying morphology. This has led to the use of a plethora of small-angle scattering models including Teubner–Strey<sup>32</sup> (Figure 3d), Deby–Beuche<sup>6,33</sup> (Figure 3e,h), polydisperse spheres with Schultz distribution<sup>14</sup> (Figure 3f), and even combinations of these (Figure 3b,c).<sup>9,31</sup> Differences in both the raw data and its interpretation have led to a significant range of deduced PCBM agglomerate sizes and length scales of P3HT/PCBM phase separation, making it difficult to understand the effect either may have on device operation.

Although discrepancies are abundant in the literature, scattering methods have made enormous contributions to the

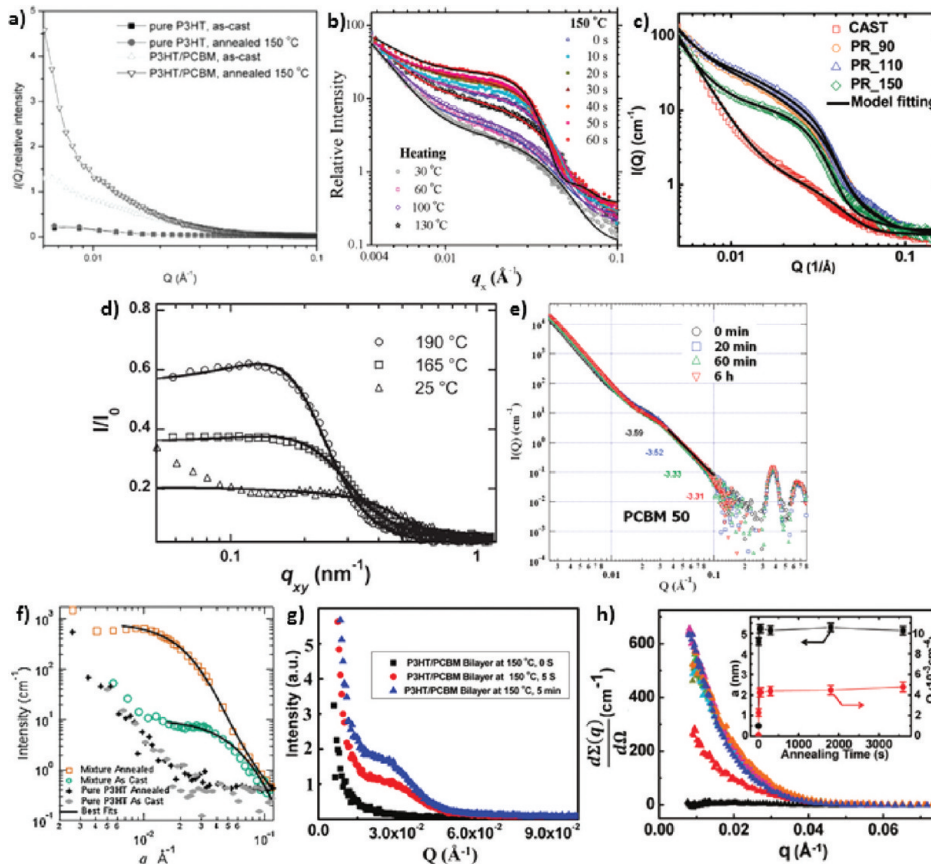


**Figure 3.** Examples of small-angle scattering studies. Small-angle scattering using (a–d) X-rays and (e–h) neutrons. X-ray scattering profiles correspond to thin films measured on PEDOT/PSS-coated silicon substrates, except for (a) and (b), which measured films on bare silicon. Neutron measurements correspond to (e) drop-cast blend films, (f,h) stacks of individually cast blend films, and (g) stacks of multiple laminated bilayers. Chlorobenzene is the typical solvent for both X-ray and neutron studies, except for (e) where dichloromethane was used. Panel (a) is taken from ref 30, adapted with permission from Wiley, copyright 2008. Panels (b–e) are taken from refs 9, 31, 32, and 33, respectively. Panel (f) is taken from ref 14, adapted with permission from APS, copyright 2010. Panels (g) and (h) are taken from refs 23 and 6, respectively.

knowledge of film morphology. GIWAXS has contributed a definitive understanding of the existence, characteristics, and positive effect of pure P3HT crystallites on performance in P3HT/PCBM devices. Small-angle scattering in the form of GISAXS and SANS has additionally demonstrated an increase of phase separation with annealing. Finally, time evolution and in situ measurements have revealed the dynamics of morphology during processing. Eliminating the discrepancies presented above, though, will require a more coherent approach to sample preparation and interpretation of the data.

**Energy-Filtered Electron Microscopy.** The varied interpretations of reciprocal space information from scattering experiments has contributed to the abundance of representations of the morphology of P3HT/PCBM devices. Real space information via microscopy techniques provides complementary information to scattering experiments but has also produced variable results. Transmission electron microscopy (TEM) is a powerful tool well suited to probe device morphology, and this technique has been a key method in guiding the debate on the nature of the material phases and their organization in OPV devices. One drawback for the technique is that the contrast between phases in a standard bright-field image is poor. This is due to the similarity of electron density between the components, unless one species is highly crystallized as, for example, low-molecular-weight P3HT ( $M_w < 20$  kDa), which is known to crystallize readily but results in OPV devices with poor PCE.

In studies using low-molecular-weight P3HT, the fiber-like P3HT crystals observed previously in atomic force microscopy images were revealed.<sup>36,37</sup> What morphology existed between the crystals and how relevant the imaged morphology was to high-performance devices remained unknown. One study using low-voltage (100 kV), high-resolution TEM microscopy<sup>38</sup> was able to discern both P3HT and PCBM crystals along with a disorganized matrix and suggested the possibility of up to four material phases in the active layer. Crucially, the sample preparation involved sonication of the prepared films in dichloromethane. However, dichloromethane is a preferential solvent for PCBM, as mentioned above. The droplet-like PCBM domains and crystallites seen in the TEM study, therefore, were possibly caused by the special sample processing used and again highlight the need for careful consideration of sample preparation.

To enhance material contrast, energy-filtered TEM (EFTEM) is increasingly employed, which only uses electrons with characteristic energy losses to image the sample.<sup>32,39–41</sup> The electron energy loss spectra (EELS) in Figure 4a demonstrate that adequate material contrast between P3HT and PCBM can be obtained, although damage to the optical electronic structure (2–7 eV) occurs.<sup>18</sup> Using the two energies exhibiting the highest respective contrast, two phases (pure P3HT crystals and an amorphous mixed phase) were reported in BHJ films with efficiencies “greater than 2% PCE”.<sup>40</sup> Subsequently, an advanced

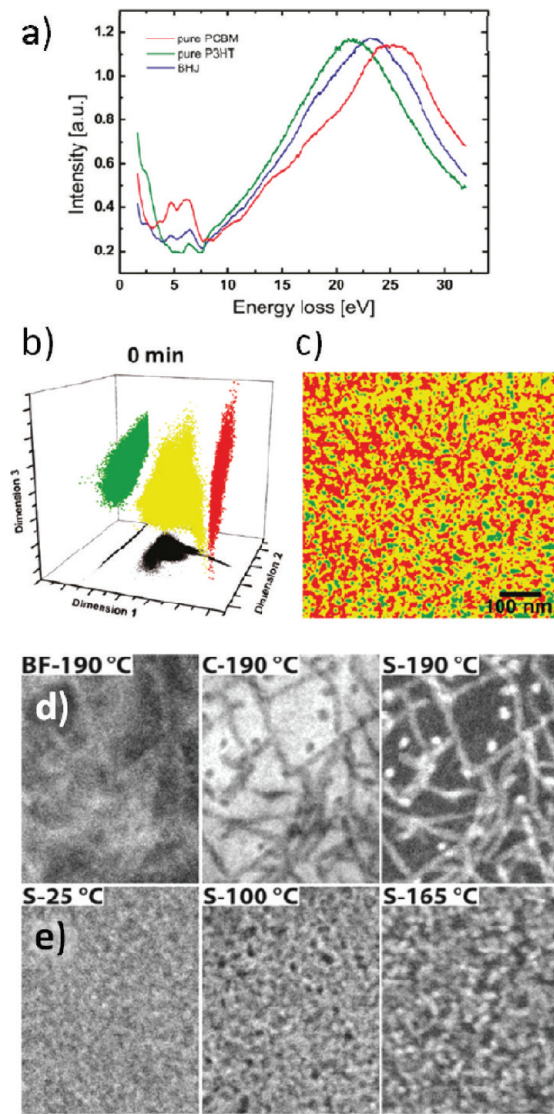


**Figure 4.** Examples of energy-filtered TEM characterization. (a) Normalized EELS demonstrating the source of contrast between P3HT and PCBM in the low-energy loss region. The BHJ trace represents 1:1 wt ratio blend films annealed for 2 min at 120 °C. (b) Scatter plots of the first three dimensions of the space spanned by LLE computed on electron spectroscopic images revealing three separated clusters for as-cast blends (chosen to highlight the LLE method). The green cluster is identified as pure P3HT, red pure PCBM, and yellow an amorphous mixture. (c) Cluster membership mapped back onto the images. (d) Bright-field, carbon edge, and sulfur edge EELS maps, respectively, of 1:1 wt ratio blend films annealed for 30 min. (e) Sulfur edge maps for the posted annealing temperatures as indicated. The scale bar is 200 nm. Panels (a–c) are taken from ref 39. Images (d) and (e) are taken from ref 32.

clustering algorithm known as local linear embedding (LLE) has been used to analyze a continuous series of images acquired in steps throughout the entire low-energy loss range.<sup>39</sup> This analysis displayed in Figure 4b,c identifies three distinguishable phases, which are labeled as pure P3HT, pure PCBM, and a mixed phase, in both as-cast and annealed films with devices producing 1.2 and 2.6% PCE, respectively. Assuming that radiation damage can be demonstrably mitigated, future work using this technique will certainly involve the extension to 3D tomography, which will help to deconvolve vertical heterogeneities projected through the traditional transmission experiment.

Another powerful EFTEM method involves using the core loss electrons at constituent elemental edges. The corresponding signal can be quantified and used to compute local compositions and map the 2D nanoscale morphology. Using this method, Kozub and co-workers were able to delineate the temperature-dependent morphology in P3HT/PCBM blend films.<sup>32</sup> P3HT crystals embedded in a mixed phase (Figure 4d,e) consisted of nodular morphologies at low temperatures, transforming into fibrillar morphologies just below the melting temperature of the P3HT crystals. Only P3HT crystals and a mixed amorphous phases were reported for any temperature. However, it is uncertain whether the additional dosage required to image with elemental core-loss electrons would cause morphological changes in the films.

*Evidence for a Mixed Amorphous Phase.* As indicated in the compositional EFTEM study, a major paradigm shift has occurred in the past 2 years regarding the molecular-scale organization of the absorbing layer. Until recently, the pure phase–discrete interface BHJ has been the canonical backdrop behind most morphological and electronic measurements. However, early X-ray spectromicroscopy work indicated that PCBM is partially miscible in P3HT.<sup>10</sup> The analysis in this study used electronic, bound-state resonances that give rise to molecular-orbital-specific X-ray absorption fine structure, allowing for clear and quantitative molecular species identification. Obtained with a scanning transmission X-ray microscope (STXM), Fickian composition profiles in the plane of the film were measured near PCBM crystals, which act as a sink for the molecular PCBM in the film. Notably, the limiting fullerene composition near the crystals was measured to be nonzero and interpreted to correspond to the composition of the binodal.<sup>10</sup>

Until recently, the pure phase–discrete interface BHJ model has been the canonical backdrop behind most morphological and electronic measurements.

Inspired by the initial spectromicroscopy work and using similar methods, we subsequently measured the partial miscibility of the fullerene with P3HT with high precision.<sup>11</sup> Because as-cast blend films are typically created in a nonequilibrium, highly mixed state, annealing is critical to improving the morphology and achieving phase separation and purification. Although equilibrium might not be reached in actual devices for which morphologies could be metastable, the thermodynamic limit of phase composition can put a lower limit on the achievable phase purity in actual devices. Upon aggressive annealing of P3HT/PCBM blend films, large PCBM crystals form, depleting the surrounding region of PCBM, as seen in Figure 5a. The measured composition of the matrix between these PCBM crystals reveals 15–20 wt % fullerene in the amorphous portions of P3HT, assuming a degree of crystallization in regio-regular (RR) P3HT of roughly 50%. The PCBM concentration additionally increases as a function of temperature (Figure 5b). Complementary to this demixing measurement, a qualitative mixing measurement was also undertaken in the same study by annealing P3HT/PCBM bilayers and characterizing the effects with dynamic secondary ion mass spectrometry (DSIMS). Results from the bilayers

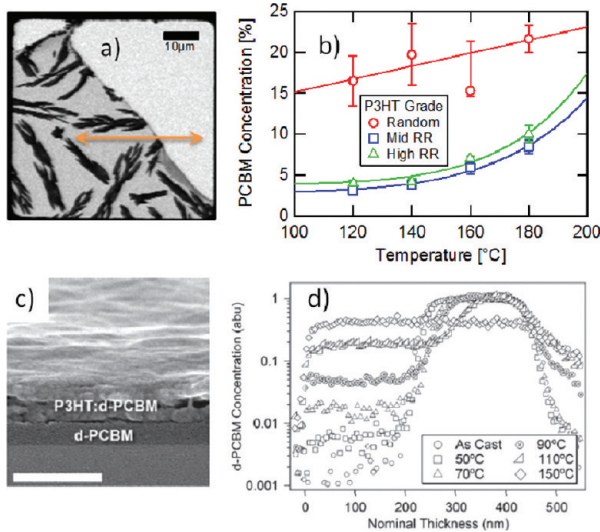


**Figure 5.** Evidence of PCBM miscibility and interdiffusion in P3HT. (a) STXM image of a blend film annealed to equilibrium acquired at 284.4 eV. Dark regions are PCBM crystals, and the light top right corner is a filmless area. The arrow designates a typical area used to generate a spectrum of the PCBM/PCBM matrix of the film. (b) Temperature-dependent residual PCBM concentration averaged over amorphous and crystalline P3HT regions of the matrix. (c) Cross-sectional SEM images of a P3HT/d-PCBM bilayer on a silicon wafer annealed at 70 °C. (d) Normalized DSIMS profiles of  $^2\text{H}$  in bilayer samples annealed for 5 min at different temperatures. Images (a) and (b) are taken from ref 11. Images (c) and (d) are taken from ref 12, adapted with permission from Wiley, copyright 2011.

demonstrated clear interdiffusion of the polymer and fullerene after only 5 min of annealing at 150 °C.

A more thorough and sensitive DSIMS study of interdiffusion of P3HT/PCBM bilayers also revealed miscibility and fast interdiffusion.<sup>12,23</sup> Figure 5c shows SEM images of a well-defined bilayer, which becomes one indistinguishable layer upon annealing. DSIMS confirmed this effect quantitatively and revealed interdiffusion even at temperatures as low as 50 °C (Figure 5d). PCBM mobility at such low temperature shows that the creation of a BHJ is a very dynamic process and may also have important implications for device stability. Other studies using similar methods agreed with these results.<sup>6,23</sup> Numerous studies are measuring miscibility using a variety of techniques that include SANS<sup>14,33</sup> and energy-filtered TEM<sup>32</sup> in addition to DSIMS and X-ray microscopy.

PCBM miscibility in P3HT has quickly become a consistent observation.

**Table 1. Manufacturer-Provided Polymer Properties of P3HT Batches Used in the Comparative Miscibility Study**

product	$M_w$ [kDa]	PDI	RR
Rieke 4002	50–60	1.8–2.2	93–95%
Merck KGaA EE	54.2	2.3	94.2%
Plextronics OS 2100	45–65	<2.0	>98%

**Material Variability and Effect on Miscibility.** In order to probe for possible sources of discrepancies found in the literature, we extended our previous miscibility study to compare the miscibility measured in similar P3HT polymers obtained from different suppliers. Here, the aim is to apply precisely the same methods in sample preparation and experiment to probe for differences in a material that should have the same or nearly identical properties. We chose three sources for P3HT: Rieke Metals Inc., Merck KGaA, and Plextronics. Their basic properties as provided by the manufacturer are listed in Table 1. Although the P3HT from Plextronics has very high regioregularity, all three materials have similar molecular weights and polydispersities. Each batch of P3HT was blended with PCBM from Nano-C (different batches) in P3HT/PCBM weight ratios of 1:1 and 1:2 and spin-cast from anhydrous chlorobenzene (Sigma Aldrich) onto sodium polystyrene

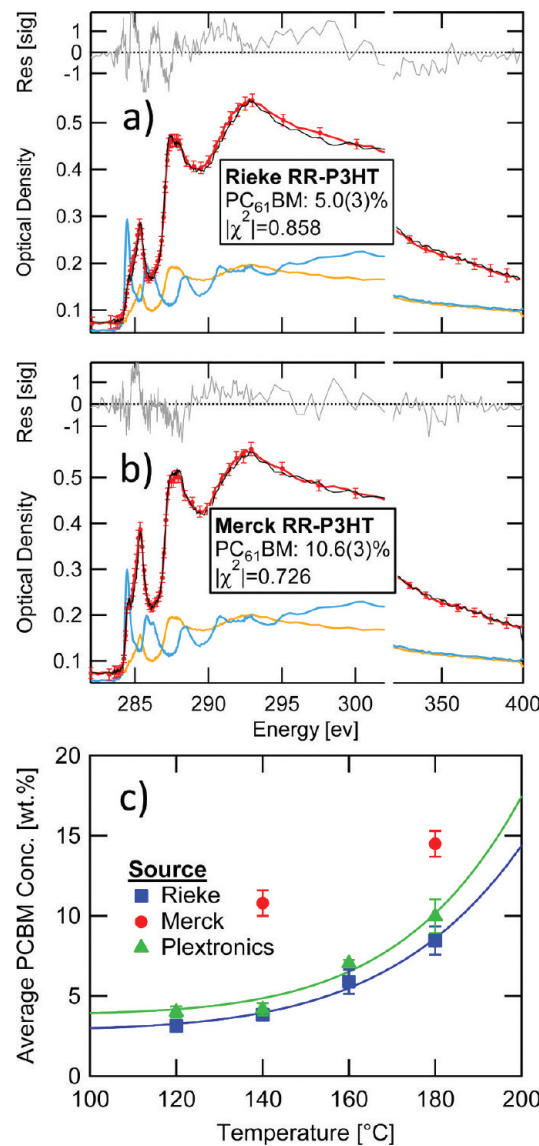


**Figure 6.** Manufacturer-dependent miscibility study. (a,b) Least-squares fits to Rieke- and Merck-sourced blend films, respectively, annealed at 140 °C until equilibrium. Red curves are data, black are fits, and blue and orange are the pure reference spectra (plotted on an independent y-axis). Gray curves are residuals calculated as (fit-data)/uncertainty. (c) Miscibility phase diagram for the three P3HT batches. Lines are guides for the eye.

sulfonate (NaPSS)-coated glass substrates. Each film was annealed under identical conditions, measured with the same STXM (different points in time), and analyzed with the same methods, all by the same researcher as in the previous study.<sup>11</sup>

Figure 6 presents the results of this comparative study. Example fits of a composition measurement on a Rieke P3HT and a Merck P3HT film are shown in Figure 6a,b and demonstrate the high quality of the fits. The resulting PCBM compositions are very precise, with only 0.3 wt % uncertainties using full error propagation on all aspects of the measurement. Surprisingly, the fullerene composition between the Rieke- and Merck-sourced samples disagree considerably. Approximately twice the fullerene content is measured in the Merck-sourced P3HT as compared with Rieke. This is remarkable as the manufacturer specifications on these two materials are nearly identical.

In addition to the different composition, we also measured a significant difference in average polymer orientation, likely arising from a difference in average crystal orientation. As described in our previous work,<sup>11</sup> the transmission near-edge X-ray absorption fine structure (NEXAFS) analysis utilized is also sensitive to the preferential orientation of the P3HT molecules relative to the substrate by virtue of the angular dependence of NEXAFS and the use of linearly polarized photons. The difference in molecular orientation can be seen qualitatively in the data, where the P3HT  $\pi^*$  resonance at 285.3 eV is more intense in the Merck-sourced material than in that from Rieke. The fits to the pure respective source materials showed that the aromatic planes of the Merck P3HT are much more aligned edge-on to the substrate than those of the Rieke P3HT. Clearly, different morphologies are arising within these two films even under identical treatment.

The results from redundant measurements on multiple films and varying initial conditions are compiled and displayed in Figure 6c. As expected and previously demonstrated,<sup>11</sup> varying the thickness or substrate surface did not affect the composition measured in the equilibrium film. Here, the disagreement of miscibility between the Merck material and the others is stark, with the Merck P3HT containing significantly more PCBM at both temperatures studied. It should be noted that these PCBM concentrations are averaged over both amorphous and pure P3HT crystalline phases as they cannot be distinguished in the STXM. Studies in the literature have reported P3HT crystallinity to range from 40 to 60%. Accounting for this would increase the actual fullerene miscibility of the amorphous portion to be between 10 and 25 wt %, in nominal agreement with noncrystallizing regiorandom P3HT.<sup>11</sup> For the Merck P3HT, PCBM crystals did not readily nucleate in 1:1 wt ratio blends. Only 1:2 wt ratio blends phase separated readily, a behavior which is consistent with the higher miscibility measured.

Because the level of P3HT crystallinity was not investigated in the Merck blend films, it cannot be ruled out as a factor behind the difference that we measure here. A lower level of crystallinity in the Merck P3HT than the others allowing for larger amorphous regions could, however, only partially explain the higher PCBM concentration. Overall, the discrepancy could be caused by either a batch-to-batch fluctuation in polymer regioregularity not reported by the manufacturer, effects of the molecular weight distribution not captured by the polydispersity index, or impurities (organic or otherwise) in either the polymer or fullerene. Regardless of the origin, this difference strongly suggests that morphological differences exist in blend films of the same materials from different suppliers and is likely a major contributing factor to the lack of convergence of

device performance seen in the P3HT/PCBM system, as shown in Figure 1b. If materials containing the same manufacturer-posted polymeric properties result in either a different miscibility or a different level of crystallinity given the same preparation conditions, device performance from these films cannot be expected to be the same. Actual measurements on independently optimized devices using different P3HT batches are required to fully test this hypothesis, however. Similarly, variations in properties of PCBM batches also need to be assessed.

*Equilibrium Considerations on Morphology and Stability.* Apart from batch-to-batch variations, the fundamental measurements of polymer–fullerene miscibility here and in the literature can help reveal insights into device morphology and the stability of that morphology. For example, the measurement of ~15 wt % PCBM miscibility in the presence of PCBM crystals will have significant consequences for devices for which crystals are not typically seen. In the recent core loss-based EFTEM work by Kozub and co-workers,<sup>32</sup> a PCBM concentration of 55 vol % was measured in the regions between P3HT crystals in their films annealed at 190 °C for 30 min, much higher than would be thought possible with a 15 wt % fundamental miscibility. This suggests that the PCBM concentration in devices is likely in a metastable state, which, in conjunction with the mobility of PCBM observed at temperatures as low as 50 °C, will pose hazards to device lifetime, especially if operated in a high-temperature environment such as a rooftop in sun-rich, southern latitudes.

Phase diagrams derived from differential scanning calorimetry (DSC) measurements support the existence of such a metastable state. Measurements of the P3HT/PCBM Flory–Huggins interaction parameter  $\chi = 0.86 \pm 0.09$  from melting point depression has allowed the calculation of the free energy of mixing of P3HT in a PCBM “solvent” using a device-relevant polymer ( $M_w = 53$  kDa with PDI = 1.9).<sup>32</sup> This results in a calculated spinodal of 58 vol % PCBM with P3HT with a  $M_w = 50$  kDa. At a higher PCBM concentration, an amorphous P3HT/PCBM system would be spontaneously unstable. Our measurements of approximately 15 wt % concentration of PCBM in the amorphous P3HT of comparable  $M_w$  correspond to a new equilibrium established in the presence of the PCBM crystals. PCBM concentrations between these two limits correspond to a metastable system. Given that typical mixtures for devices have a PCBM concentration of 40–50 wt %, device morphologies are metastable even in the absence of P3HT crystallization unless P3HT of sufficiently low  $M_w$  is used. Crystallization during annealing will push the PCBM concentration in the remaining amorphous P3HT further into the two-phase region of the phase diagram, ultimately leading to the formation of large PCBM crystals. This effect was also seen in an earlier DSC study conducted without a full understanding of the cause.<sup>42</sup>

Such a metastable state is a significant hazard to device lifetime and suggests that the presence of PCBM crystallization at any size is something to be avoided in these devices. The rapid diffusion of PCBM in P3HT even at relatively low temperatures,<sup>10,12,23</sup> along with this significant gap between metastable and equilibrium states, suggests that any nucleated PCBM crystals would rapidly grow to micrometer-sized crystals at elevated temperature, depleting the surrounding matrix and making nanoscale PCBM crystals in freshly prepared devices highly unlikely. This is confirmed by most GIWAXS studies.

The existence of a metastable state in devices also has implications for the question of a third PCBM agglomerate phase. For device operation, what is necessary is a continuous percolation pathway of all electrons through PCBM molecules

out of the device. At 15 wt % PCBM in amorphous P3HT as measured near equilibrium, this condition will certainly not be met. At 55 vol % measured using EFTEM in actual devices, percolation pathways are not only certain but are likely to be highly interconnected. At this concentration, a third agglomerate phase might not aid in creating better electron-transport pathways to the electrodes. Quite the contrary, they could deplete the mixed phase, making electron traps from isolated PCBM molecules more likely. This would be revealed in devices as an increase in nongeminate recombination, a loss mechanism not seen to significantly hamper the photocurrent of P3HT/PCBM devices.<sup>43</sup> Thus, either amorphous PCBM agglomerates do not occur in these devices or their presence is small enough to constitute little importance for the device performance.

A metastable state is a significant hazard to device lifetime and suggests that the presence of PCBM crystallization at any size is something to be avoided in these devices.

DSC work additionally provides evidence for the driving force of phase separation.<sup>32</sup> Because typical mixtures of 1:1 wt ratio are only 42 vol % PCBM in actual devices, this is below the DSC-derived spinodal and precludes spinodal decomposition as a mechanism for phase separation. Only after P3HT crystallizes is the PCBM concentration in the remaining amorphous P3HT in the unstable two-phase region, resulting in nucleated PCBM crystals that rapidly grow to micrometer sizes. This finding is in agreement with previous work showing higher degrees of PCBM crystallization as P3HT regioregularity (and therefore P3HT crystallization) is increased.<sup>19</sup> The effect was also seen in our work on miscibility, in which initial PCBM levels in both the Merck RR-P3HT and Rieke RRa-P3HT were required to be above 50 wt % before PCBM crystallization occurred. However, time-dependent simultaneous scattering and diffraction<sup>9</sup> showed some kind of phase separation prior to crystallization, which, given the composition and thermodynamics, would most likely correspond to nucleation and growth events. In the end, the questions that we have discussed here are clearly yet to be answered in definite terms. Only through work where care is exercised both in the experiment and in the sample preparation, and with materials that have proven to yield high-performance devices, can such definitive answers be found. Yet, in all work on device morphology, issues of miscibility must be considered.

**Outlook.** Even though a clear and concrete morphological picture of P3HT/PCBM is still evolving, significant leaps forward will only occur when the aforementioned characterization techniques are conducted in tandem with measurements of device performance. An example of this synergy is in advanced scanning probe techniques,<sup>44</sup> where electro-optical function and morphology can be simultaneously investigated, thus linking measurements of photocurrent extraction with morphological characterization. New, higher-performing mate-

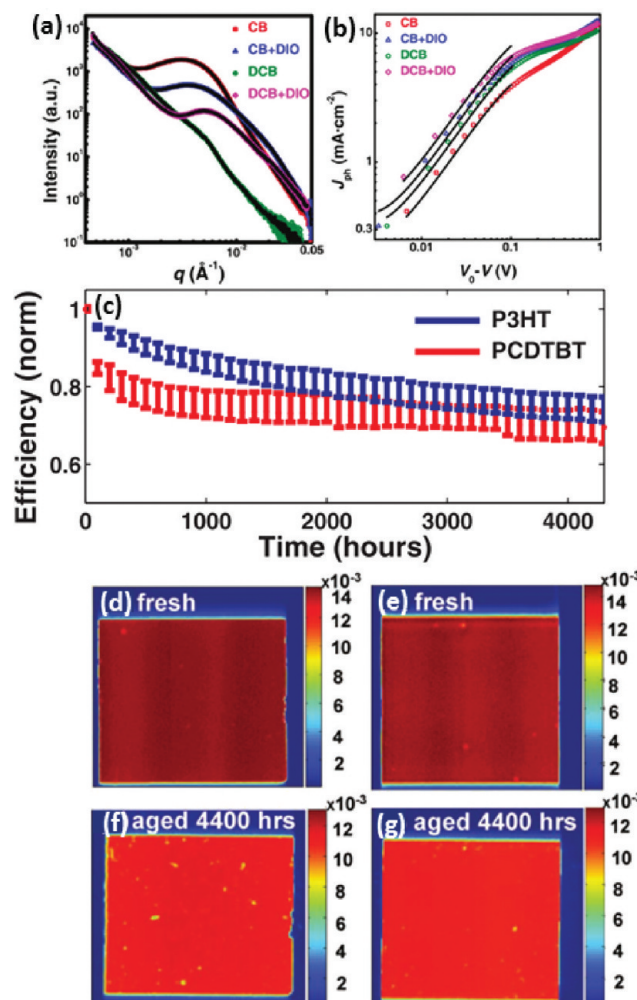


**Figure 7.** High-performance materials and lifetime considerations. (a) Resonant soft X-ray scattering of PTB7/PC<sub>61</sub>BM thin films cast from different solvents and (b) photocurrent device measurements. (c) The lifetime of solar cells with PCDTBT/PC<sub>71</sub>BM device twice that of P3HT/PC<sub>61</sub>BM devices (based on the slope after the burn-in period). Laser-beam-induced current maps of (d,f) P3HT/PC<sub>61</sub>BM and (e,g) PCDTBT/PC<sub>71</sub>BM devices before and after aging experiments. Device active areas are  $\sim 13 \text{ mm}^2$ . Panels (a) and (b) are taken from ref 15. Images (c–g) are taken from ref 48, adapted with permission from Wiley, copyright 2011.

rials have additionally benefited from a comprehensive examination because the morphological features prove to be quite different from those found in P3HT/PCBM. For example, the highest performing polymer–fullerene combination involves a copolymer with alternating ester-substituted thieno[3,4-*b*]thiophene and benzodithiophene units (PTB7), mixed with PC<sub>71</sub>BM for which efficiencies nearing 8.4% have been reported.<sup>1</sup> In order to achieve high performance for this system, solvent additives that induce and control PCBM segregation or agglomeration are used.<sup>45,46</sup> The effect of additives is shown in Figure 7a, depicting resonant soft X-ray scattering (R-SoXS) profiles for PTB7/PC<sub>61</sub>BM films cast using different solvent mixtures.<sup>15</sup> The relatively new technique of R-SoXS used here utilizes X-rays tuned to molecular resonances to enhance material contrast over other sources of scattering such as surface roughness.<sup>47</sup> Length scales from several nanometers to several micrometers are probed, and the morphology that corresponds to the casting solvent that yields

the greatest number of dissociated excitons at open-circuit (Figure 7b) can be determined. Unfortunately, use of PC<sub>61</sub>BM in this particular study instead of PC<sub>71</sub>BM resulted in a reduction in device performance by nearly a factor of 2, calling into question whether the characterized hierarchical morphology is truly relevant to high-performance devices with PCE  $\approx$  8%. Even so, this work appropriately combines advanced morphological characterization with measured device performance, eliminating significant sources of error such as material and processing variability.

As performance of freshly fabricated devices approaches economically viable efficiencies, the field is beginning to also focus on device lifetime and stability, where equilibrium considerations are likely to be important. For systems like P3HT/PC<sub>61</sub>BM, for which performance is optimized by creating and exploiting a metastable morphology, degradation in performance can occur by morphological evolution over time. This is demonstrated in Figure 7c for P3HT/PC<sub>61</sub>BM and compared to a relatively new, higher-performing polymer, poly[9'-hepta-decanyl-2,7-carbazole-*alt*-5,5-(4',7'-di-2-thienyl-2',1',3'-benzothiadiazole)] (PCDTBT) blended with PC<sub>71</sub>BM. Following ISOS standardized lifetime measurements,<sup>49</sup> the lifetime for P3HT/PC<sub>61</sub>BM was measured to be  $\sim$ 3 years, while that of PCDTBT/PC<sub>71</sub>BM was over double that value.<sup>48</sup> In this study, laser-beam-induced current maps before and after aging for P3HT/PC<sub>61</sub>BM (Figure 7d,f) and PCDTBT/PC<sub>71</sub>BM (Figure 7e,g) devices showed a greater population of defects that cause shorting in the P3HT/PC<sub>61</sub>BM, which are potentially due to the formation of fullerene microcrystals. Here again, equilibrium properties of the materials may explain the differences in lifetime. For instance, PCDTBT does not exhibit the same level of crystallinity as P3HT.<sup>50</sup> Recent comparisons of PC<sub>61</sub>BM to PC<sub>71</sub>BM miscibility have additionally shown that the C<sub>70</sub>-based fullerene has a much higher equilibrium composition in some conjugated polymers.<sup>51</sup> This suggests a PC<sub>71</sub>BM-enriched amorphous phase might be closer to thermodynamic equilibrium than PC<sub>61</sub>BM-rich phases and thus be more stable. Therefore, along with PCE, morphological stability linked to the materials' miscibility and proximity of the device phase composition to that of equilibrium will become an important figure of merit for OPV devices.

Overall, tremendous effort has been exerted to characterize the morphology of OPV active layers, with P3HT/PCBM being the most ubiquitous system investigated. While the traditional BHJ picture of a binary system described by discrete interfaces between pure domains in BHJ OPVs has been shown to be in need of revision, questions about actual morphologies still abound that are complicated by variations between material batches and in the processing conditions utilized. Advanced characterization of device morphology will be most useful when applied to samples consistent with optimized, high-performing devices.

**Advanced characterization of device morphology will be most useful when applied to samples consistent with optimized, high-performing devices.**

We have also shown that the typical material parameters provided by suppliers ( $M_w$ , PDI, regioregularity, and purity) are either not a complete set determining device morphological characteristics, inaccurate, or both. Therefore, materials' parameters need to be more fully characterized and systematically varied to study their impact on morphology and performance. Advances might also be accelerated by use of round-robin modalities that share materials, samples, and expertise between researchers involved in material synthesis, device characterization, and complementary morphological exploration alike. Lastly, due to the propensity of PCBM to crystallize, long-term stability in PCBM-based systems should be improved through the use of crystallizable donor materials for which PCBM is highly miscible in the amorphous regions. The miscibility of materials as measured by a variety of methods is thus an important indicator alongside PCE to be considered and manipulated when gauging the economic viability of a particular materials system.

## AUTHOR INFORMATION

### Corresponding Author

\*E-mail: harald\_ade@nscu.edu.

### Biographies

**Brian A. Collins** received a B.A. in physics from Gustavus Adolphus College in St. Peter, MN, in 2003 and M.S. and Ph.D. degrees from the University of North Carolina at Chapel Hill in 2005 and 2009 also in physics. He is currently a postdoctoral researcher in Harald Ade's lab.

**John R. Tumbleston** earned a B.S. from Elon University in physics in 2006. In 2008 and 2011, he received physics M.S. and Ph.D. degrees from the University of North Carolina at Chapel Hill. Currently, he is a postdoctoral researcher in the Ade lab.

**Harald Ade** received a physics Ph.D. from SUNY at Stony Brook in 1990 and has held appointments at NCSU since 1992. He is developing and using novel soft X-ray characterization tools. H. Ade received (amongst others) an R&D100 Award (1990), NYI Award (1994), and the K. F. J. Heinrich Award (2000) and is a Fellow of the APS and the AAAS.

## ACKNOWLEDGMENTS

The authors gratefully thank Dean DeLongchamp, Thomas P. Russell, and U-Ser Jeng for fruitful discussions. Christopher R. McNeill is acknowledged for supplying the P3HT used in the extended miscibility measurement. The work was supported by the U.S. Department of Energy, Office of Science, Basic Energy Science, Division of Materials Science and Engineering under Contract DE-FG02-98ER45737. STXM data were acquired at beamline 5.3.2.2 at the Advanced Light Source, Berkeley, which is supported by the Director, Office of Science, Office of Basic Energy Sciences, of the U.S. Department of Energy under Contract No. DE-AC02-05CH11231.

## REFERENCES

- (1) He, Z.; Zhong, C.; Huang, X.; Wong, W.-Y.; Wu, H.; Chen, L.; Su, S.; Yong, C. Simultaneous Enhancement of Open-Circuit Voltage, Short-Circuit Current Density, and Fill Factor in Polymer Solar Cells. *Adv. Mater.* **2011**, *23*, 4636–4643.
- (2) Halls, J. J. M.; Walsh, C. A.; Greenham, N. C.; Marseglia, E. A.; Friend, R. H.; Moratti, S. C.; Holmes, A. B. Efficient Photodiodes from Interpenetrating Polymer Networks. *Nature* **1995**, *376*, 498–500.

- (3) Yu, G.; Heeger, A. J. Charge Separation and Photovoltaic Conversion in Polymer Composites with Internal Donor/Acceptor Heterojunctions. *J. Appl. Phys.* **1995**, *78*, 4510–4515.
- (4) Coakley, K. M.; McGehee, M. D. Conjugated Polymer Photovoltaic Cells. *Chem. Mater.* **2004**, *16*, 4533–4542.
- (5) Günes, S.; Neugebauer, H.; Sariciftci, N. S. Conjugated Polymer-Based Organic Solar Cells. *Chem. Rev.* **2007**, *107*, 1324–1338.
- (6) Chen, D.; Nakahara, A.; Wei, D.; Nordlund, D.; Russell, T. P. P3HT/PCBM Bulk Heterojunction Organic Photovoltaics: Correlating Efficiency and Morphology. *Nano Lett.* **2011**, *11*, 561–567.
- (7) Agostinelli, T.; Lilliu, S.; Labram, J. G.; Campoy-Quiles, M.; Hampton, M.; Pires, E.; Rawle, J.; Bikondoa, O.; Bradley, D. D. C.; Anthopoulos, T. D.; et al. Real-Time Investigation of Crystallization and Phase-Segregation Dynamics in P3HT:PCBM Solar Cells During Thermal Annealing. *Adv. Funct. Mater.* **2011**, *21*, 1701–1708.
- (8) Vaynzof, Y.; Kabra, D.; Zhao, L.; Chua, L. L.; Steiner, U.; Friend, R. H. Surface-Directed Spinodal Decomposition in Poly[3-hexylthiophene] and C61-Butyric Acid Methyl Ester Blends. *ACS Nano* **2011**, *5*, 329–336.
- (9) Wu, W.-R.; Jeng, U.-S.; Su, C.-J.; Wei, K.-H.; Su, M.-S.; Chiu, M.-Y.; Chen, C.-Y.; Su, W.-B.; Su, C.-H.; Su, A.-C. Competition between Fullerene Aggregation and Poly(3-hexylthiophene) Crystallization upon Annealing of Bulk Heterojunction Solar Cells. *ACS Nano* **2011**, *5*, 6233–6243.
- (10) Watts, B.; Belcher, W. J.; Thomsen, L.; Ade, H.; Dastoor, P. C. A Quantitative Study of PCBM Diffusion during Annealing of P3HT:PCBM Blend Films. *Macromolecules* **2009**, *42*, 8392–8397.
- (11) Collins, B. A.; Gann, E.; Guignard, L.; He, X.; McNeill, C. R.; Ade, H. Molecular Miscibility of Polymer–Fullerene Blends. *J. Phys. Chem. Lett.* **2010**, *1*, 3160–3166.
- (12) Treat, N. D.; Brady, M. A.; Smith, G.; Toney, M. F.; Kramer, E. J.; Hawker, C. J.; Chabinyc, M. L. Interdiffusion of PCBM and P3HT Reveals Miscibility in a Photovoltaically Active Blend. *Adv. Energy Mater.* **2011**, *1*, 82–89.
- (13) Parnell, A. J.; Cadby, A. J.; Mykhaylyk, O. O.; Dunbar, A. D. F.; Hopkinson, P. E.; Donald, A. M.; Jones, R. A. L. Nanoscale Phase Separation of P3HT PCBM Thick Films As Measured by Small-Angle X-ray Scattering. *Macromolecules* **2011**, *44*, 6503–6508.
- (14) Kiel, J. W.; Eberle, A. P. R.; Mackay, M. E. Nanoparticle Agglomeration in Polymer-Based Solar Cells. *Phys. Rev. Lett.* **2010**, *105*, 168701.
- (15) Chen, W.; Xu, T.; He, F.; Wang, W.; Wang, C.; Strzalka, J.; Liu, Y.; Wen, J.; Miller, D. J.; Chen, J.; et al. Hierarchical Nanomorphologies Promote Exciton Dissociation in Polymer/Fullerene Bulk Heterojunction Solar Cells. *Nano Lett.* **2011**, *11*, 3707–3713.
- (16) Chang, L.; Lademann, H. W. A.; Bonekamp, J.-B.; Meerholz, K.; Moulé, A. J. Effect of Trace Solvent on the Morphology of P3HT:PCBM Bulk Heterojunction Solar Cells. *Adv. Funct. Mater.* **2011**, *21*, 1779–1787.
- (17) Dang, M. T.; Hirsch, L.; Wantz, G. P3HT:PCBM, Best Seller in Polymer Photovoltaic Research. *Adv. Mater.* **2011**, *23*, 3597–3602.
- (18) Pfannmöller, M.; Flügge, H.; Benner, G.; Wacker, I.; Kowalsky, W.; Schröder, R. R. Visualizing Photovoltaic Nanostructures with High-Resolution Analytical Electron Microscopy Reveals Material Phases in Bulk Heterojunctions. *Synth. Met.* **2011**, DOI: 10.1016/j.synthmet.2011.09.011.
- (19) Woo, C. H.; Thompson, B. C.; Kim, B. J.; Toney, M. F.; Fréchet, J. M. J. The Influence of Poly(3-hexylthiophene) Regioregularity on Fullerene-Composite Solar Cell Performance. *J. Am. Chem. Soc.* **2008**, *130*, 16324–16329.
- (20) Ruderer, M. A.; Guo, S.; Meier, R.; Chiang, H.-Y.; Körstgens, V.; Wiedersich, J.; Perlich, J.; Roth, S. V.; Müller-Buschbaum, P. Solvent-Induced Morphology in Polymer-Based Systems for Organic Photovoltaics. *Adv. Funct. Mater.* **2011**, *21*, 3382–3391.
- (21) Mihailescu, V. D.; Xie, H.; de Boer, B.; Koster, L. J. A.; Blom, P. W. M. Charge Transport and Photocurrent Generation in Poly(3-hexylthiophene):Methanofullerene Bulk-Heterojunction Solar Cells. *Adv. Funct. Mater.* **2006**, *16*, 699–708.
- (22) Koster, L. J. A.; Wienk, M. M.; Maturová, K.; Janssen, R. A. J. Quantifying Bimolecular Recombination Losses in Organic Bulk Heterojunction Solar Cells. *Adv. Mater.* **2011**, *23*, 1670–1674.
- (23) Chen, D.; Liu, F.; Wang, C.; Nakahara, A.; Russell, T. P. Bulk Heterojunction Photovoltaic Active Layers via Bilayer Interdiffusion. *Nano Lett.* **2011**, *11*, 2071–2078.
- (24) Treat, N. D.; Shuttle, C. G.; Toney, M. F.; Hawker, C. J.; Chabinyc, M. L. In Situ Measurement of Power Conversion Efficiency and Molecular Ordering During Thermal Annealing in P3HT:PCBM Bulk Heterojunction Solar Cells. *J. Mater. Chem.* **2011**, *15*, 224–15231.
- (25) Schmidt-Hansberg, B.; Sanyal, M.; Klein, M. F. G.; Pfaff, M.; Schnabel, N.; Jaiser, S.; Vorobiev, A.; Müller, E.; Colsmann, A.; Scharfer, P.; et al. Moving Through the Phase Diagram: Morphology Formation in Solution Cast Polymer–Fullerene Blend Films for Organic Solar Cells. *ACS Nano* **2011**, *5*, 8579–8590.
- (26) Verploegen, E.; Mondal, R.; Bettinger, C. J.; Sok, S.; Toney, M. F.; Bao, Z. Effects of Thermal Annealing Upon the Morphology of Polymer–Fullerene Blends. *Adv. Funct. Mater.* **2010**, *20*, 3519–3529.
- (27) Nieuwendaal, R. C.; Snyder, C. R.; Kline, R. J.; Lin, E. K.; VanderHart, D. L.; DeLongchamp, D. M. Measuring the Extent of Phase Separation in Poly-3-hexylthiophene/Phenyl-C61-Butyric Acid Methyl Ester Photovoltaic Blends with <sup>1</sup>H Spin Diffusion NMR Spectroscopy. *Chem. Mater.* **2010**, *22*, 2930–2936.
- (28) Lilliu, S.; Agostinelli, T.; Pires, E.; Hampton, M.; Nelson, J.; Macdonald, J. E. Dynamics of Crystallization and Disorder during Annealing of P3HT/PCBM Bulk Heterojunctions. *Macromolecules* **2011**, *44*, 2725–2734.
- (29) Gomez, E. D.; Barreau, K. P.; Wang, H.; Toney, M. F.; Loo, Y.-L. Correlating the Scattered Intensities of P3HT and PCBM to the Current Densities of Polymer Solar Cells. *Chem. Commun.* **2011**, *47*, 436–438.
- (30) Chiu, M.-Y.; Jeng, U.-S.; Su, C.-H.; Liang, K. S.; Wei, K.-H. Simultaneous Use of Small- and Wide-Angle X-ray Techniques to Analyze Nanometerscale Phase Separation in Polymer Heterojunction Solar Cells. *Adv. Mater.* **2008**, *20*, 2573–2578.
- (31) Liao, H.-C.; Tsao, C.-S.; Lin, T.-H.; Chuang, C.-M.; Chen, C.-Y.; Jeng, U.-S.; Su, C.-H.; Chen, Y.-F.; Su, W.-F. Quantitative Nanoorganized Structural Evolution for a High Efficiency Bulk Heterojunction Polymer Solar Cell. *J. Am. Chem. Soc.* **2011**, *133*, 13064–13073.
- (32) Kozub, D. R.; Vakhshouri, K.; Orme, L. M.; Wang, C.; Hexemer, A.; Gomez, E. D. Polymer Crystallization of Partially Miscible Polythiophene/Fullerene Mixtures Controls Morphology. *Macromolecules* **2011**, *44*, 5722–5726.
- (33) Yin, W.; Dadmun, M. A New Model for the Morphology of P3HT/PCBM Organic Photovoltaics from Small-Angle Neutron Scattering: Rivers and Streams. *ACS Nano* **2011**, *5*, 4756–4768.
- (34) Ayzner, A. L.; Tassone, C. J.; Tolbert, S. H.; Schwartz, B. J. Reappraising the Need for Bulk Heterojunctions in Polymer–Fullerene Photovoltaics: The Role of Carrier Transport in All-Solution-Processed P3HT/PCBM Bilayer Solar Cells. *J. Phys. Chem. C* **2009**, *113*, 20050–20060.
- (35) He, C.; Germack, D. S.; Kline, R. J.; Delongchamp, D. M.; Fischer, D. A.; Snyder, C. R.; Toney, M. F.; Kushmerick, J. G.; Richter, L. J. Influence of Substrate on Crystallization in Polythiophene/Fullerene Blends. *Sol. Energy Mater. Sol. Cells* **2011**, *95*, 1375–1381.
- (36) Zen, A.; Saphiannikova, M.; Neher, D.; Grenzer, J.; Grigorian, S.; Pietsch, U.; Asawapirom, U.; Janietz, S.; Scherf, U.; Lieberwirth, I.; et al. Effect of Molecular Weight on the Structure and Crystallinity of Poly(3-hexylthiophene). *Macromolecules* **2006**, *39*, 2162–2171.
- (37) van Bavel, S. S.; Souris, E.; de With, G.; Loos, J. Three-Dimensional Nanoscale Organization of Bulk Heterojunction Polymer Solar Cells. *Nano Lett.* **2009**, *9*, 507–513.
- (38) Beal, R. M.; Stavrinidis, A.; Warner, J. H.; Smith, J. M.; Assender, H. E.; Watt, A. A. R. The Molecular Structure of Polymer–Fullerene Composite Solar Cells and Its Influence on Device Performance. *Macromolecules* **2010**, *43*, 2343–2348.

- (39) Pfannmöller, M.; Flügge, H.; Benner, G.; Wacker, I.; Sommer, C.; Hanselmann, M.; Schmale, S.; Schmidt, H.; Hamprecht, F. A.; Rabe, T.; et al. Visualizing a Homogeneous Blend in Bulk Heterojunction Polymer Solar Cells by Analytical Electron Microscopy. *Nano Lett.* **2011**, *11*, 3099–3107.
- (40) Herzing, A. A.; Richter, L. J.; Anderson, I. M. 3D Nanoscale Characterization of Thin-Film Organic Photovoltaic Device Structures via Spectroscopic Contrast in the TEM. *J. Phys. Chem. C* **2010**, *114*, 17501–17508.
- (41) Drummy, L. F.; Davis, R. J.; Moore, D. L.; Durstock, M.; Vaia, R. A.; Hsu, J. W. P. Molecular-Scale and Nanoscale Morphology of P3HT:PCBM Bulk Heterojunctions: Energy-Filtered TEM and Low-Dose HREM. *Chem. Mater.* **2011**, *23*, 907–912.
- (42) Kim, J. Y.; Frisbie, C. D. Correlation of Phase Behavior and Charge Transport in Conjugated Polymer/Fullerene Blends. *J. Phys. Chem. C* **2008**, *112*, 17726–17736.
- (43) Dibb, G. F. A.; Kirchartz, T.; Credgington, D.; Durrant, J. R.; Nelson, J. Analysis of the Relationship between Linearity of Corrected Photocurrent and the Order of Recombination in Organic Solar Cells. *J. Phys. Chem. Lett.* **2011**, *2*, 2407–2411.
- (44) Groves, C.; Reid, O. G.; Ginger, D. S. Heterogeneity in Polymer Solar Cells: Local Morphology and Performance in Organic Photovoltaics Studied with Scanning Probe Microscopy. *Acc. Chem. Res.* **2010**, *43*, 612–620.
- (45) Liang, Y.; Xu, Z.; Xia, J.; Tsai, S.-T.; Wu, Y.; Li, G.; Ray, C.; Yu, L. For the Bright Future-Bulk Heterojunction Polymer Solar Cells with Power Conversion Efficiency of 7.4%. *Adv. Energy Mater.* **2010**, *22*, E135–E138.
- (46) Hammond, M. R.; Kline, R. J.; Herzing, A. A.; Richter, L. J.; Germack, D. S.; Ro, H.-W.; Soles, C. L.; Fischer, D. A.; Xu, T.; Yu, L.; et al. Molecular Order in High-Efficiency Polymer/Fullerene Bulk Heterojunction Solar Cells. *ACS Nano* **2011**, *5*, 8248–8257.
- (47) Swaraj, S.; Wang, C.; Yan, H.; Watts, B.; Lüning, J.; McNeill, C. R.; Ade, H. Nanomorphology of Bulk Heterojunction Photovoltaic Thin Films Probed with Resonant Soft X-ray Scattering. *Nano Lett.* **2010**, *10*, 2863–2869.
- (48) Peters, C. H.; Sachs-Quintana, I. T.; Kastrop, J. P.; Beaupré, S.; Leclerc, M.; McGehee, M. D. High Efficiency Polymer Solar Cells with Long Operating Lifetimes. *Adv. Energy Mater.* **2011**, *1*, 491–494.
- (49) Reese, M. O.; Gevorgyan, S. A.; Jørgensen, M.; Bundgaard, E.; Kurtz, S. R.; Ginley, D. S.; Olson, D. C.; Lloyd, M. T.; Morville, P.; Katz, E. A.; et al. Consensus Stability Testing Protocols for Organic Photovoltaic Materials and Devices. *Sol. Energy Mater. Sol. Cells* **2011**, *95*, 1253–1267.
- (50) Beiley, Z. M.; Hoke, E. T.; Noriega, R.; Dacuña, J.; Burkhard, G. F.; Bartelt, J. A.; Salleo, A.; Toney, M. F.; McGehee, M. D. Morphology-Dependent Trap Formation in High Performance Polymer Bulk Heterojunction Solar Cells. *Adv. Energy Mater.* **2011**, *1*, 954–962.
- (51) Collins, B. A.; Li, Z.; McNeill, C. R.; Ade, H. Fullerene-Dependent Miscibility in the Silole-Containing Copolymer PSBTBT-08. *Macromolecules* **2011**, DOI: 10.1021/ma201883a.